# Solid lipid nanoparticles self-assembled from spray dried microparticles

Brenda Sanchez-Vazquez,[a] Jong Bong Lee,[b] Margarita Strimaite,[a] Asma Buanz,[a] Russell Bailey,[c] Pavel Gershkovich,[b] George Pasparakis[a] and Gareth R. Williams[a]*

[a] UCL School of Pharmacy, University College London, 29-39 Brunswick Square, London WC1N 1AX, UK.

[b] Centre for Biomolecular Sciences, University of Nottingham, University Park, Nottingham NG7 2RD, UK.

[c] School of Engineering and Materials Science, Queen Mary University of London, Mile End Road, London, E1 4NS, UK.

* Corresponding authors. Email: g.pasparakis@ucl.ac.uk; g.williams@ucl.ac.uk

**Abstract**

We report the self-assembly of anti-cancer drug-loaded solid lipid nanoparticles (SLNs) from spray dried microparticles comprising poly(vinylpyrrolidone) (PVP) loaded with glyceryl tristearate (GTS) and either indomethacin (IMC) or 5-fluorouracil (5-FU). When the spray dried microparticles are added to water, the PVP matrix dissolves and the GTS and drug self-assemble into SLNs. The SLNs provide a non-toxic delivery platform for both hydrophobic (indomethacin) and hydrophilic (5-fluorouracil) drugs. They show extended release profiles over more than 24 h, and in permeation studies the drug cargo is seen to accumulate inside cancer cells. This overcomes major issues with achieving local intestinal delivery of these active ingredients, in that IMC permeates well and thus will enter the systemic circulation and potentially lead to side effects, while 5-FU remains in the lumen of the small intestine and will be secreted without having any therapeutic benefit. The SLN formulations are as effective as the pure drugs in terms of their ability to induce cell death. Our approach represents a new and simple route to the fabrication of SLNs: by assembling these from spray-dried microparticles on demand, we can circumvent the low storage stability which plagues SLN formulations.

**Keywords**

Spray-drying; self-assembly; solid lipid nanoparticle; drug delivery system; stability

## 1. Introduction

Solid lipid nanoparticles (SLNs) are colloidal drug carriers of size between 50 – 400 nm which have been much explored as an alternative to emulsions, liposomes, and polymeric particles. They contain solid lipids such as fatty acids, steroids, glycerides and waxes in place of the liquid lipids which are employed for other formulations (Muller et al., 1995). SLNs are advantageous over other lipid-based systems in terms of their small size, large surface area, and high biocompatibility (owing to the low toxicity of their components) (Mehnert and Mäder, 2001). In addition, they can provide highly controlled drug delivery. There is thus great interest in the use of SLNs as drug nanocarriers (Mukherjee et al., 2009), for instance in the improvement of treatments for various types of cancer (Chen et al., 2001; Kang et al., 2010; Lee et al., 2007; Yang et al., 1999). However, there are a number of drawbacks to SLNs, including a limited drug-loading capacity and sometimes rapid expulsion of the encapsulated drug. A major problem is the commonly reported gelation of SLN dispersions, and a marked increase of their particle size upon storage owing to poor colloidal stability (Das and Chaudhury, 2011).

The most common processes for fabricating SLNs are high pressure homogenization or sonication (Mehnert and Mäder, 2001, 2012). Both involve melting the lipid and drug, followed by the formation of an emulsion by dispersing the melt into a hot aqueous surfactant solution. Subsequent cooling of the emulsion allows the solidification of the lipid, giving an aqueous dispersion of SLNs. These aqueous dispersions can then be converted into a dry powder to improve storage stability (Mehnert and Mäder, 2001, 2012). This multi-step process is time consuming and expensive however, and the use of heat can be problematic for thermally labile drugs. Alternative SLN manufacturing processes are thus much sought after (Mehnert and Mäder, 2012).

One alternative approach to SLN fabrication involves the use of polymer-based microcomposites as sacrificial templates. In this paradigm, a fast-dissolving hydrophilic matrix containing the drug and lipid as a molecular dispersion is first prepared, and then added to water. As the hydrophilic matrix takes up water, the hydrophobic components (the drug and lipid) cluster together and self-assemble into SLNs. This route has been proven viable using polymer composites generated by electrohydrodynamic (EHD) approaches, as reported by Yu *et al.* (Yu et al., 2011b). However, although EHD approaches are increasingly recognised as being scalable from the lab bench to industrial production volumes (Démuth et al., 2016; Farkas et al., 2019; Valtera et al., 2019; Vass et al., 2019), the vast majority of research on them has to date been performed at small scale, and the techniques have yet to be adopted by the pharmaceutical industry.

In contrast, the spray drying approach to preparing polymer-based composites is widely used in the pharmaceutical (and food) industries for a variety of applications (Poozesh and Bilgili, 2019; Ziaee et al., 2019). It involves rapid evaporation of the solvent from a solution, and results in spherical particles of around 1 – 5 μm in size. Spray drying has extensively explored to generate formulations of active pharmaceutical ingredients (APIs), with systems containing etravirine, ivacaftor, tacrolimus, itraconazole, and everolimus, among many others, having been reported (Newman, 2015; Ziaee et al., 2019). Typically spray dried microparticles comprise amorphous solid dispersions, offering advantages in solubility and dissolution rate over other formulation approaches.

Spray drying has also been studied for developing SLN and other nanoparticulate-based formulations. There are four different approaches that can be envisaged. In the first (Figure 1(a)), a suspension of SLNs can be spray dried into a dry reconstitutable powder. This has been reported on a number of occasions, but obstacles such as particle growth have been encountered as a consequence of the use of high temperatures and the resultant melting of the lipid phase (Salminen et al., 2019). Extensive

optimisation is also required (Xia et al., 2016). The second method uses the spray-drying technique for the top-down preparation of nanoparticle-loaded polymer microparticles, by processing suspensions of nanoparticles in a polymer solution (see Figure 1(b)). The resultant formulations have been found to have potential for the formulation of APIs for delivery by multiple administration routes (Müller et al., 2000). Both these methods require the SLNs to be prepared prior to spray drying, rendering them rather complex multi-step processes.

A potentially more interesting application of spray drying is its putative use in the bottom-up self-assembly of nanoscale objects. In the case of SLNs, this would involve processing a solution of drug, lipid, and polymer. These could either self-assemble into SLNs during the drying process (Figure 1(c)), or produce a molecular dispersion of drug and lipid in polymer (Figure 1(d)). Such bottom-up self-assembly is a much simpler route to nanoscale systems than the top-down method, and can be completed in two steps (preparation of the microparticles, and then addition of the solvent). There are several reports of the former in the literature. For instance, Pansare et al. have used this to self-assemble nanocrystals of phenytoin in a hydroxypropyl methylcellulose / poly(lactic acid)-poly(ethylene glycol) block copolymer by spray drying (Pansare et al., 2018), while Liu and co-workers have generated core/shell microparticles with a Eudragit RS shell and silica sol core (Liu et al., 2011). In both cases, complex architectures could be obtained in a single step during drying. In related work, Suhendi et al. were able to assemble silica nanoparticles and polystyrene spheres during the spray drying process (Suhendi et al., 2013), and Fatnassi combined sol-gel approaches with spray-drying to obtain drug-loaded nanostructured microparticles (Fatnassi et al., 2010).

To date, to the best of our knowledge, there are no reports in the literature of the final situation, in which a molecular dispersion is generated by spray drying and then self-assembles upon addition to water. There are also no reports of self-assembling SLNs in spray drying, despite the great benefits of these systems. In this work, we sought for the first time to self-assemble SLNs from spray dried

105 formulations. To do this, we employed the hydrophilic polymer poly(vinylpyrrolidone) (PVP), the solid
106 lipid glyceryl tristearate (GTS), and either 5-fluorouracil (5-FU) or indomethacin (IMC), two drugs with
107 potential in the treatment of colon cancer (Foley et al., 2008; Hull et al., 2003; Wang and DuBois,
108 2006). We hypothesised that the PVP-based microparticles produced could act as "proto-SLNs",
109 allowing us to produce formulations which are long-term stable and can be converted to SLNs on
110 demand.
111

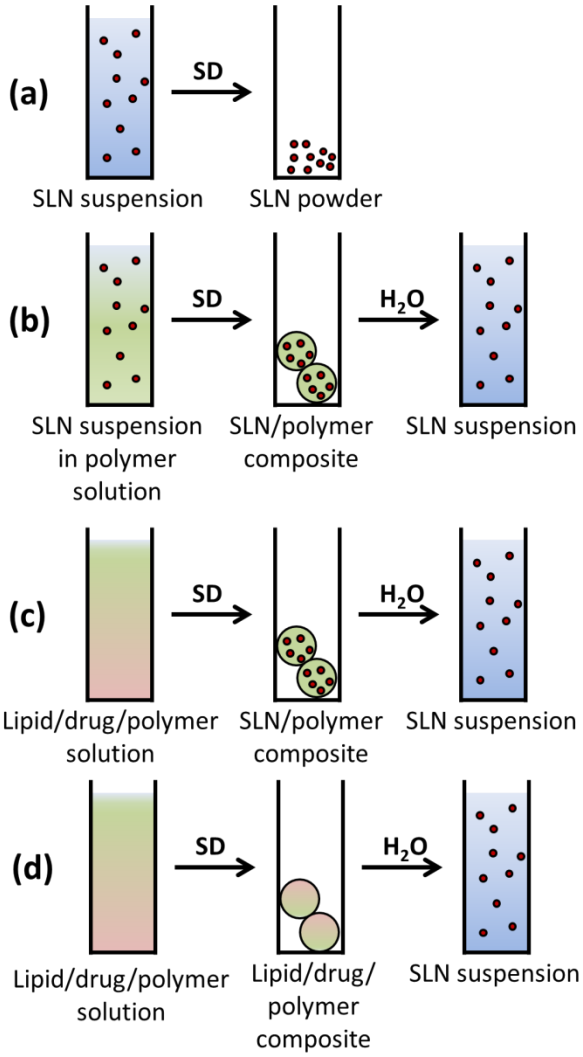


Figure 1: Schematic illustrations of the different approaches to produce drug-loaded SLN-based formulations by spray drying (SD). (a) A suspension of drug-loaded SLNs can be converted into a powder; (b) a suspension of drug-loaded SLNs in a polymer solution yields SLN/polymer composites, which can later dissolve to give free SLNs; (c) a solution of lipid, drug, and polymer can be converted into SLN-loaded polymer particles in the SD step, and again the latter can be dissolved in an aqueous medium to free the SLNs, and (d) a lipid/drug/polymer solution can be processed into a molecular dispersion composite, which then self-assembles into drug-loaded SLNs when water is added.

## 2. Materials and methods

### *2.1 Synthetic procedures*

Solutions containing indomethacin (IMC, Alfa Aesar) or 5-fluorouracil (5-FU, Sigma-Aldrich) were prepared prior to the spray drying process. These solutions were composed of the drug, polyvinylpyrrolidone (PVP, 40

kDa, Sigma-Aldrich) and glyceryl tristearate (GTS, Sigma-Aldrich). Chloroform was used as the solvent for IMC. In the case of 5-FU, the drug was fully dissolved in dimethylformamide (DMF) and then mixed with a PVP/GTS solution in chloroform for 10 min before spray drying. All solvents were from Fisher Scientific. The solutions contained final concentrations of 10 % w/v of polymer, 5 % w/v of GTS and 2.5 % w/v drug.

Spray drying was performed using a mini spray dryer (Buchi B-290, Laboratory-Technik Ltd) with a closed loop. The spray nozzle tip diameter was 0.7 mm. The inlet air temperature was 70 °C and the outlet air temperature 40–48 °C. The liquid feed rate to the dryer was 10 mL $min^{-1}$, and the flow of drying gas approximately 35 $m^3 h^{-1}$. Experiments were performed under constant process conditions. After letting the equipment cool down to below 50 °C, the dry powder was collected from the particle chamber. The material obtained was stored in a desiccator containing silica gel until required for further use. The yield from spray drying was ca. 35 % w/w.

For the self-assembly process, 10 mg of the spray dried formulations was accurately weighed, added to 10 mL of distilled water, and sonicated for 10 min to assist with the formation of SLNs. The resultant suspension was then filtered using a 0.22 µm syringe filter.

*2.2 Scanning electron microscopy*

The spray dried particles were analysed by scanning electron microscopy (SEM), which was performed using a field emission microscope (FEI Quanta 200F) connected to a secondary electron detector. Samples were adhered to a SEM stub with carbon-coated double-sided tape, and sputter coated with gold to render them conductive prior to measurement. Particle diameters were measured using the ImageJ software (National Institutes of Health). At least 100 particles were measured, and the values are reported as mean ± standard deviation (S.D.).

Focused ion beam (FIB) SEM was performed by mounting samples on adhesive carbon coated aluminium pads and coating them with carbon in a Balzers CED 030 carbon evaporator. FIB-SEM was then undertaken in a FEI Quanta 3D FEG instrument, by first sputtering the particles of interest with platinum and subsequently ablating with $Ga^{3+}$ ions.

### *2.3 Transmission electron microscopy*

One drop of the self-assembled SLN suspension was mixed with a drop of 1 % w/v aqueous uranyl acetate solution, and the resultant mixture dropped on a carbon-coated copper grid. Transmission electron microscopy (TEM) was undertaken on a JEOL KEM-2100F microscope.

### *2.4 Differential scanning calorimetry*

Thermograms were obtained on a Q2000 differential scanning calorimeter (DSC, TA Instruments). Around 2-5 mg of sample was placed in a non-hermetically sealed aluminium pan (T130425, TA Instruments). The samples were heated from 0 – 110 °C at 10°C $min^{-1}$ (to remove any adsorbed water), followed by cooling to 0 °C at 10 °C $min^{-1}$ and reheating to 200 °C, again at 10 °C $min^{-1}$. All stages were performed under a 50 mL $min^{-1}$ flow of oxygen-free nitrogen gas. The TA Universal Analysis software was used to analyse the data.

### *2.5 X-Ray diffraction*

X-ray diffraction (XRD) patterns were collected on a Rigaku Miniflex 600 diffractometer supplied with Cu Kα radiation (1.5418 Å) at 40 kV and 15 mA. Patterns were recorded over the 2θ range 3 – 40° at a speed of 5° $min^{-1}$.

### *2.6 IR spectroscopy*

IR spectra were obtained from 4000 to 650 $cm^{-1}$ on a Perkin Elmer Spectrum 100 instrument.

176 *2.7 Dynamic light scattering*

177 The size of the self-assembled SLNs was quantified using dynamic light scattering (DLS) on a Zetasizer Nano
178 ZS instrument (Malvern Instruments). Each formulation was dispersed in distilled water at a concentration
179 of 1 mg $mL^{-1}$, and a disposable polystyrene cuvette employed for sizing. The experiment was performed in
180 triplicate, with each suspension being prepared three times. To investigate the stability of the SLNs, the
181 suspension was stored and further DLS measurements collected after 6 months.

182

183 *2.8 Entrapment efficiency*

184 The entrapment efficiency (EE) was calculated as follows. 3 mL of the self-assembled SLNs were loaded into
185 a filter centrifuge tube (Amicon Ultra-15, 3000 MWCO, Merck Millipore) and centrifuged at 9500 rpm for 10
186 min at 25 °C, with acceleration and brake set to 9. After centrifugation, the filtrate was recovered and
187 analysed by UV spectroscopy (Cary 100 spectrophotometer, Agilent Technologies) at 240 nm (IMC) and 265
188 nm (5-FU). %EE was calculated using Equation 1:

189

190 $$\%EE = \frac{W_{total\ drug} - W_{free\ drug}}{W_{total\ drug}}\ x\ 100$$

191 Equation 1

192 $W_{total\ drug}$ represents the overall mass of drug in the formulation, $W_{free\ drug}$ is the mass of drug present in the
193 supernatant.

194

195 *2.9 Drug release studies*

196 5 mL of the aqueous SLN suspension was transferred into a cellulose dialysis bag (Fisher Scientific, 3500
197 MWCO, volume/cm=1.5). The latter was then placed in an autoclave bottle containing 50 mL of phosphate
198 buffered saline (PBS; pH 6.8) or fasted state simulated intestinal fluid, FaSSIF (Biorelevant) at 37 °C, and
199 stirred at 80 rpm. 2 mL aliquots were withdrawn periodically and replaced with the same volume of fresh
200 preheated media. The aliquots were filtered (0.22 µm filter) and the drug concentration quantified by UV-vis
201 spectroscopy (Cary 100 spectrophotometer, Agilent Technologies). Experiments were performed in triplicate

and data are presented as mean ± S.D. Control experiments were performed in PBS using both suspensions of the raw drug particles and solutions of the APIs.

### *2.10 Cell culture*

The colorectal adenocarcinoma cell line Caco-2 (ATCC HTB-37) was employed for *in vitro* studies. Cells were maintained at 37 °C, under 5 % $CO_2$, in Dulbecco's modified Eagle's medium (DMEM-HG; Gibco) supplemented with penicillin-streptomycin (1 % v/v) and L-glutamine (1 % v/v) solutions, non-essential amino acid solution (1 % v/v) (all Life Technologies), and 10 % v/v heat-inactivated fetal bovine serum (Gibco) (termed "complete DMEM"). Cells were passaged until required for further studies. This process involved a treatment with 0.05 % trypsin-EDTA solution. The passage numbers for the viability experiments were between 26 and 30.

The human dermal fibroblast (HDF) cell line was purchased from Life Technologies (lot 771555). The cells were maintained at 37 °C, under a 5 % $CO_2$ atmosphere, in Dulbecco's modified Eagle's medium-high glucose (DMEM-HG) supplemented with 10 % (v/v) heat-inactivated fetal bovine serum (Gibco), 2 mM $L^{-1}$ glutamine, 1 % v/v MEM non-essential amino acids, gentamicin solution (100 µg $mL^{-1}$) and amphotericin B solution (0.25 µg $mL^{-1}$) (all Life Technologies). Cells were passaged when a confluence of 70 – 80 % was reached through treatment with 0.05 % trypsin-EDTA solution. The passage number for the viability experiments was between 20 and 25.

For viability tests, Biolite 24 well multidish clear plates (ThermoFisher) were used. The seeding density was 5 x $10^4$ cells $mL^{-1}$, and each well contained 1 mL of media. The formulations to be tested were dispersed in complete DMEM (1 mg $mL^{-1}$), filtered through a 0.22 µm filter, and 180 µL of the resultant SLN suspension was added to the wells of the plate. The cells were incubated with the dissolved formulations for 48 h. Cell viability was determined using the Alamar Blue™ cell viability assay (ThermoFisher). The reagent was prepared following the manufacturer's instructions, and added to the culture plates with a reagent volume

equal to the volume of cell culture medium present in each well. After addition, the plate was incubated for 60 minutes at 37 °C and 5 % $CO_2$ before absorbance at 570 nm and 600 nm was read using a SpectraMax M2e spectrophotometer (Molecular Devices). The viability of the cells was calculated using the Equation 2.

$$\%\ viability\ = \frac{100 \times \left(A_{570,treated\ cells} - A_{600,treated\ cells}\right)}{\left(A_{570,untreated\ cells} - A_{600,untreated\ cells}\right)}$$

Equation 2

*2.11 Permeation assays*

Permeation assays were performed following a previously reported protocol (Lee et al., 2017). Caco-2 cells were grown in complete DMEM in a Falcon® 24-multiwell insert system plate (Corning) for 21 days, changing the medium every 2 days. The seeding density was 3.75 x $10^4$ cells $cm^{-2}$. On the day of the assay, the Caco-2 monolayer was washed twice with transport buffer (Hanks Balanced Salt Solution supplemented with 10 mM 4-(2-hydroxyethyl)-1-piperazineethanesulfonic acid and with the pH adjusted to 7.4). The cells were left to equilibrate for 30 min at 37 °C. The assay was initiated when the donor solution (containing 200 µM of the drug) was placed on the apical side of the monolayer, and samples of 250 µL were withdrawn from the basal side at different time points over 2 h. Fresh buffer was supplied at each time to maintain a constant volume. The transepithelial electrical resistance (TEER) was measured before and after the experiment to assess the integrity of the monolayer. All experiments were performed in triplicate.

The apparent permeability coefficient (Papp) was calculated using the Equation 3.

$$Papp = \left(\frac{dQ}{dt}\right) \times \frac{1}{AC_0}$$

Equation 3

Where dQ/dt is the steady state flux (µmol $s^{-1}$) and $C_0$ is the initial concentration in the donor chamber (µM), A represents the effective filter area of each well ($cm^2$).

Samples obtained from the permeation studies were subjected to a liquid-liquid extraction using ethyl acetate as the organic solvent. After the addition of ethyl acetate (2 mL) to each sample, they were vortexed for 2 min and then left to separate and for the organic layer to evaporate. The latter was accelerated using a stream of air.

### *2.12 High performance liquid chromatography*

High performance liquid chromatography (HPLC) was performed on the permeation study samples using previously published and validated methods (Nassim et al., 2002). The residue from liquid-liquid extraction was first reconstituted in an appropriate mobile phase. The IMC mobile phase comprised 0.5 % v/v aqueous orthophosphoric acid, methanol, and acetonitrile (all Fisher) at volume ratios of 40: 20: 40. For 5-FU the mobile phase was acetonitrile: water (10: 90 v/v). For both analyses, a Luna C18 column (Phenomenex) was utilised with an injection volume of 10 µL. IMC experiments were undertaken at a flow rate of 2 mL $min^{-1}$, and 5-FU chromatograms recorded at a flow rate of 1 mL $min^{-1}$ (Tsvetkova, 2012).

### *2.13 Stability studies*

The stability of the SLNs was assessed by measuring their size immediately after fabrication, and after storage at room temperature for 6 months. The spray-dried microparticles were also stored under the same conditions, and a fresh batch of SLNs assembled from them after 6 months. The size of the SLNs was determined by DLS in each case.

### *2.14 Statistical analysis*

Size data obtained from DLS were analysed using a one tailed Student's t-test. The level of significance was set at $p < 0.05$. Data from cell culture experiments were statistically analysed using the MiniTab17 Software. The statistical significance of differences was evaluated by one-way ANOVA using Dunnett simultaneous 95% CIs tests.

## 3. Results and discussion

### *3.1 Spray drying*

The production of PVP/GTS/drug particles by spray drying was found to be facile (see Figure 2). Three formulations were prepared, comprising PVP/GTS alone (SD-PVP-GTS), and PVP and GTS with IMC (SD-IMC) or 5-FU (SD-5FU). All three formulations comprise spherical particles with an average size of 6.61 ± 4.16 µm for SD-PVP-GTS, 7.15 ± 4.39 µm for SD-IMC, and 5.78 ± 4.44 µm for SD-5FU (PDIs: 0.63, 0.61 and 0.77, respectively). A wide range of particle sizes have clearly formed, and in addition a few very fine fibres (due to the high molecular weight of the polymer used) can be seen in all cases.

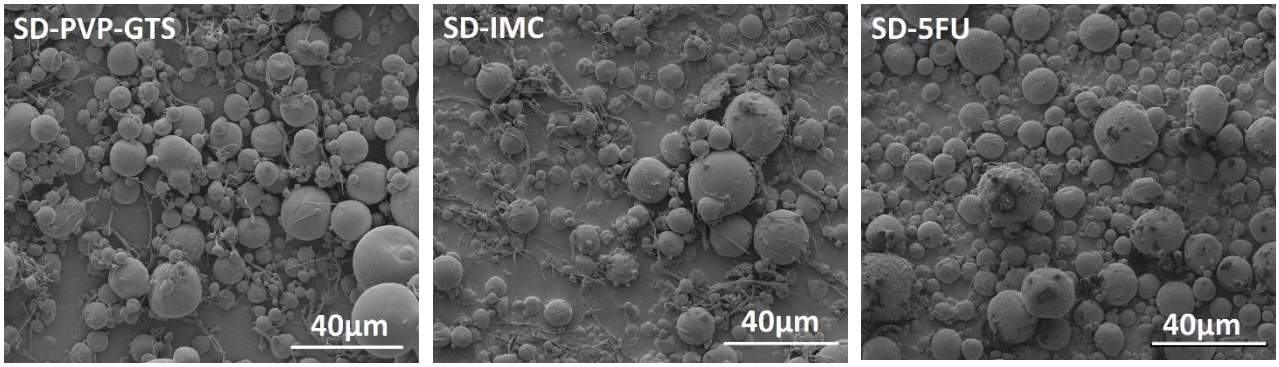


Figure 2: SEM images of the spray-dried formulations. SD-PVP-GTS contains PVP and GTS alone, while SD-IMC and SD-5FU also include a drug (indomethacin or 5-fluorouracil respectively).

The physical form of the components in the microparticles was explored using differential scanning calorimetry (DSC) and X-ray diffraction (XRD). DSC thermograms are given in Figure 3. PVP is clearly amorphous: no melting peaks can be seen. The IMC data display a sharp endotherm at 161.7 °C due the melting of the γ-form of IMC (Dupeyrón et al., 2013). 5-FU similarly shows a sharp melting endotherm at 284 °C, again in agreement with the literature (Kalantarian et al., 2010). This confirms both to be crystalline solids. In the case of GTS, there are two endotherms (at 49 and 60 °C) and one exotherm (51.2 °C). The first endotherm indicates the melting of α-GTS, followed by recrystallisation (exotherm) to β-GTS and then melting of the latter (second endotherm) (Singh et al., 1999a, b). GTS is thus also a crystalline material. In the case of the formulations, thermograms could not be obtained

at temperatures above 180 °C because PVP carbonizes at 200 °C. Thus, the 5-FU melt lies outside the

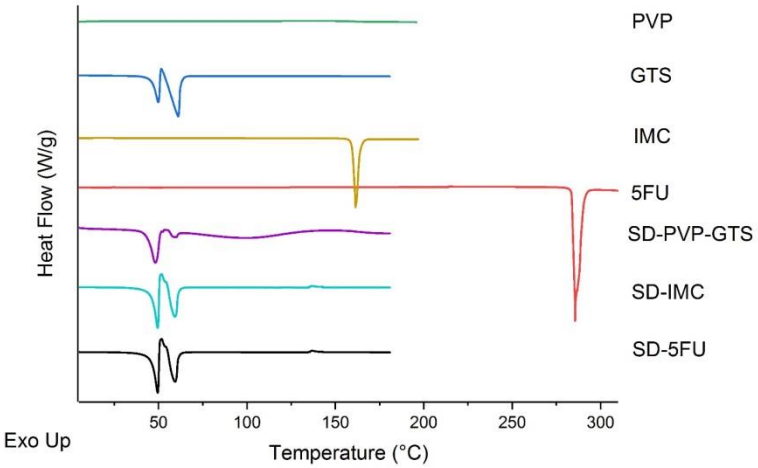


heating range measured. The thermograms of the formulations show the same behaviour as GTS, with the presence of crystalline GTS clearly present. There is no IMC melting endotherm visible in SD-IMC, and thus the drug is amorphous here.

Figure 3: DSC thermograms showing the second heating cycle.

XRD data are shown in Figure 4. IMC is a crystalline material, with numerous distinct Bragg reflections present between 10-30°, and the pattern matches that reported for the γ-form of IMC (Dupeyrón et al., 2013). 5-FU also exhibits a number of Bragg reflections, confirming its crystalline nature. GTS shows a Bragg reflection at 21.4°, indicating the semi crystalline nature of the material (Lutton, 1945). No sharp peaks are observed in the PVP pattern, with only slight haloes at around 12 and 21°, confirming it to be amorphous. Two broad halos can be observed in SD-PVP-GTS, SD-IMC and SD-5-FU, one of them being a broad hump characteristic of PVP while the peak at 21.4° corresponds to GTS. After spray drying, no Bragg reflections corresponding to the APIs can be seen in SD-IMC and SD-5-FU. They are thus amorphously distributed in the SD particles. The spray drying process results in a rapid transition from solution to solid, and thus often results in predominately amorphous

materials for small molecules because there is no time for crystallisation to take place (Takeuchi et al., 2005).

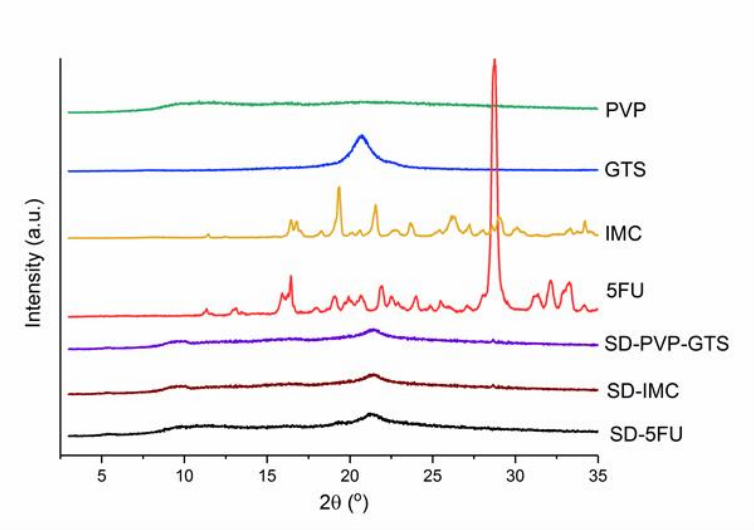


Figure 4: XRD patterns of the raw materials and formulations.

IR spectra of the raw materials and formulations can be found in Figure 5. The PVP spectrum contains two weak broad bands at 3200 – 3600 $cm^{-1}$ and 2800 – 3000 $cm^{-1}$, indicating O-H and C-H stretching. The O-H stretching is believed to be due to the water adsorbed by the polymer. The peak at 1660 $cm^{-1}$ corresponds to C=O stretching. IMC displays peaks between 1580 – 1620 $cm^{-1}$ from aromatic C=C stretching, C=O stretching at 1680 $cm^{-1}$, and bands at 1261 $cm^{-1}$ (asymmetric aromatic O-C stretching), 1086 $cm^{-1}$ (symmetric aromatic O-H stretching) and between 2800 – 3000 $cm^{-1}$ (C-H stretching). For 5-FU, the characteristic bands are at 1429 – 1600 $cm^{-1}$ (C=N and C=C ring stretching vibrations), 1720 $cm^{-1}$ (C=O stretching), 1345 $cm^{-1}$ (pyridine vibrations) and 2989 $cm^{-1}$ (N-H stretching). GTS show two strong peaks at 2917 and 2850$cm^{-1}$ and a shoulder at 2960 $cm^{-1}$ (C-H stretching). C=O stretching from the ester group manifests in a strong peak at 1740 $cm^{-1}$. Considering the formulations, the major peaks from GTS at ca. 1740, 2917 and 2850 $cm^{-1}$ can be observed. Other than these peaks, the spectra of the formulations are very similar to that of PVP. The characteristic carboxylate bands of IMC are shifted to lower wavenumbers and overlap with the carbonyl band of

PVP at 1660 $cm^{-1}$ in SD-IMC. Similar observations are noted in the SD-5-FU spectrum. In both cases, this suggests the presence of interactions between the drug and polymer. This is strongly indicative that after spray drying, the composites obtained comprise homogeneous molecular dispersions of drug-in-polymer.

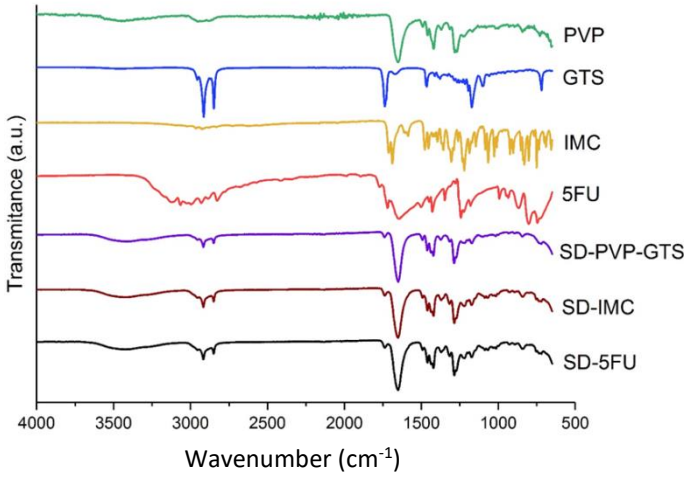


Figure 5: IR spectra.

### *3.2 SLN self-assembly*

When the microparticles are added to water, smaller spherical objects of around 100 nm in size are observed in TEM images (Figure 6 and Supplementary Information, Figure S1). The products of this process are denoted SLN-PVP-GTS (generated from the spray dried PVP/GTS formulation), SLN-IMC and SLN-5FU (formed from the IMC and 5-FU-loaded formulations respectively). These are SLNs, and the images very closely resemble those previously reported in the literature (Ali et al., 2017; Kumar and Randhawa, 2015; Vieira et al., 2016; Yuan et al., 2014). From the images, the SLNs appear to be monolithic in nature, with no evidence for any core/shell morphology or phase separation. DLS (Figure 7) revealed the size of the particles to be 219 ± 9 nm for SLN-IMC, 251 ± 25 nm for SLN-5FU and 876 ± 99 nm for SLN-PVP-GTS. The particle size is relatively homogeneous for all the drug-loaded samples, but the presence of aggregates is apparent with SLN-PVP-GTS. After filtration through a 0.22 µm membrane, the sizes are reduced to 156 ± 3 nm, 134 ± 4 nm and 142 ± 3 nm for SLN-PVP-GTS,

SLN-IMC and SLN-5FU, respectively. The PDIs after filtration are 0.10 ± 0.01 and 0.14 ± 0.01 for SLN-IMC and SLN-5FU respectively. Any undissolved lumps and aggregates larger than 0.22 µm are removed after filtration, and thus the size distributions of the SLNs become narrower.

The formation of the SLNs can be attributed to the separation of hydrophilic and hydrophobic components of the microparticles. When the PVP-based microparticles are added to water, they will rapidly take up water, swell and start to dissolve. As they do so, the hydrophobic GTS and the drug will tend to aggregate together, to minimise contact with the aqueous phase. This results in the formation of nanoparticles comprising GTS and the drug forming as the PVP matrix is wetted, disaggregates and dissolves (Yu et al., 2011a).

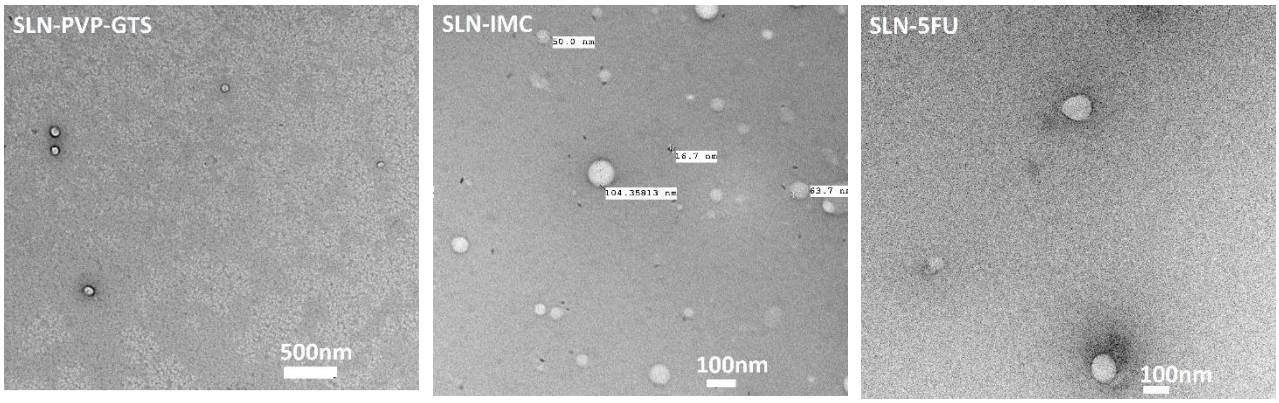


Figure 6: TEM images of the self-assembled SLNs. SLN-PVP-GTS are generated from the spray dried PVP/GTS formulation, while SLN-IMC and SLN-5FU are formed from the indomethacin and 5-fluoruracil-loaded formulations respectively.

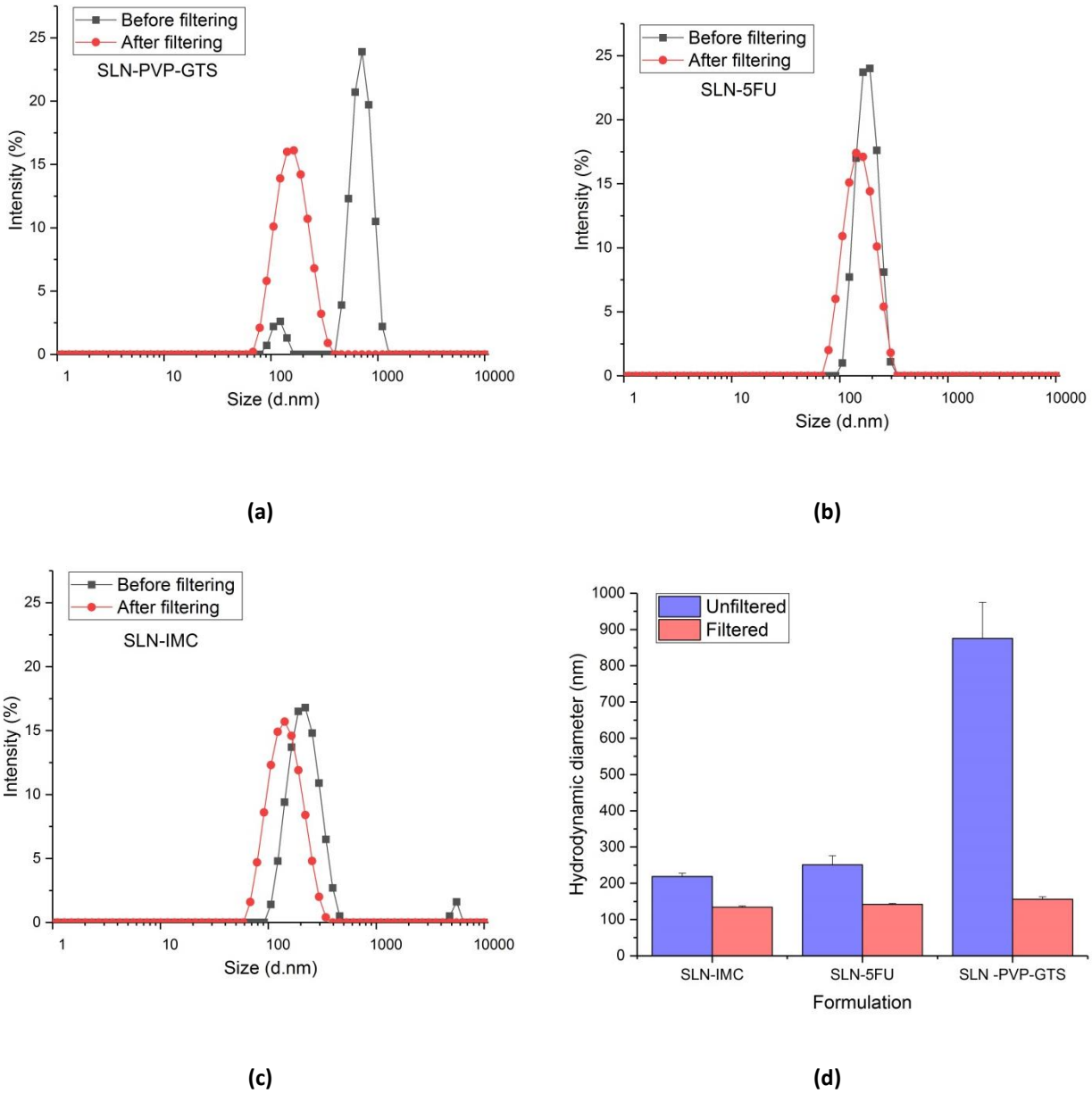


369 Figure 7: DLS data on the SLNs, with raw data shown for (a) SLN-PVP-GTS; (b) SLN-5FU; and, (c) SLN-IMC, together with (d) a summary
370 of the particle sizes obtained. Data are shown both before and after filtration with a 0.22 µm syringe filter.

371 The theoretical drug loading in the formulations was 14.3 % w/w. Upon addition of SD-IMC and SD-
372 5FU to water, the entrapment efficiency (EE) into SLNs was determined to be 86.2 ± 4.8 % and 64.9
373 ± 16.7 % respectively. The EE is influenced by the properties of both the lipid and the API, and thus
374 the higher EE for SLN-IMC can be explained by the more hydrophobic nature of IMC. These EE values
375 are similar to those reported in the literature (Du et al., 2010; Hippalgaonkar et al., 2013). The drug
376 loading of the SLNs is 12.3 ± 0.7 % for SLN-IMC and 9.3 ± 2.4 % for SLN-5FU.

### *3.3 Internal structure*

The internal structure of the spray dried SD-IMC material was explored with FIB-SEM (Figure 8). The images show the particles to have a hollow structure, with some small dark objects observable in the shell and some larger particles present in the core. The former are of the size of the SLNs, at ca. 100 – 200 nm, but they are few in number. The SLN components GTS and IMC form 43 % of the particle mass, and given the relative volumes each spray dried particle should contain of the order of $10^4$ SLNs. The FIB-SEM data thus suggest that, although some SLNs may have self-assembled during the spray drying process, there is no evidence for the formation of significant numbers of nanoparticles during this procedure. The images in Figure 8 indicate that there is some phase separation in the spray-dried microparticles, which is consistent with the observation of semi-crystalline GTS in XRD and DSC. However, the fact that large numbers of SLNs cannot be observed inside the structure suggests that the situation depicted in Figure 1(d) is most likely to be correct. This is the first time that such a self-assembly process has been noted from spray dried microparticles.

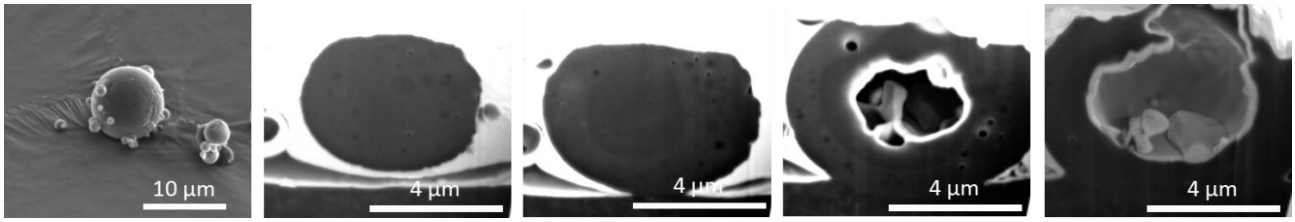


Figure 8: FIB-SEM images of SD-IMC.

### *3.4 Drug release*

In this work, we sought to make formulations to treat cancers in the small intestine, ideally for oral delivery. The mean pH from the small intestine to the colon varies between 6.6 and 7.5 (Evans et al., 1988). Therefore, *in vitro* drug release experiments were performed using phosphate buffered saline (PBS) at pH 6.8, and also fasted state simulated intestinal fluid (FASSIF). The latter is reported to provide a more accurate prediction of the *in vivo* release profile of the drug than simple PBS (Vertzoni

et al., 2005). To elucidate the effect of the dialysis tubing, we explored the effect of loading either solution of the drug or a suspension of drug particles in the tubing (Figure S2). For 5-FU, there is very little difference between the profiles, since the API dissolves quickly into the aqueous medium. In contrast, the low solubility of IMC leads to distinct differences between the solution and suspension experiment. In both cases, the drug solutions transfer rapidly through the dialysis tubing, and thus it can be concluded that the tubing does not have any retarding effect on drug release: once the API is in solution, it passes through the membrane into the bulk medium.

The SLN release plots are given in Figure 9. When using PBS, it can be observed that there was a burst release of the entrapped IMC and 5-FU from the formulations in the first 7 h, and after this period slow release over 48 h. More rapid release was seen for the pure drugs. The behaviour of SLN-IMC is very similar to this in FASSIF, while SLN-5FU is much slower to release its drug cargo than in PBS. After 48 h in FASSIF, approx. 70 % of the incorporated indomethacin and 55 % of the 5-FU is released from the formulations.

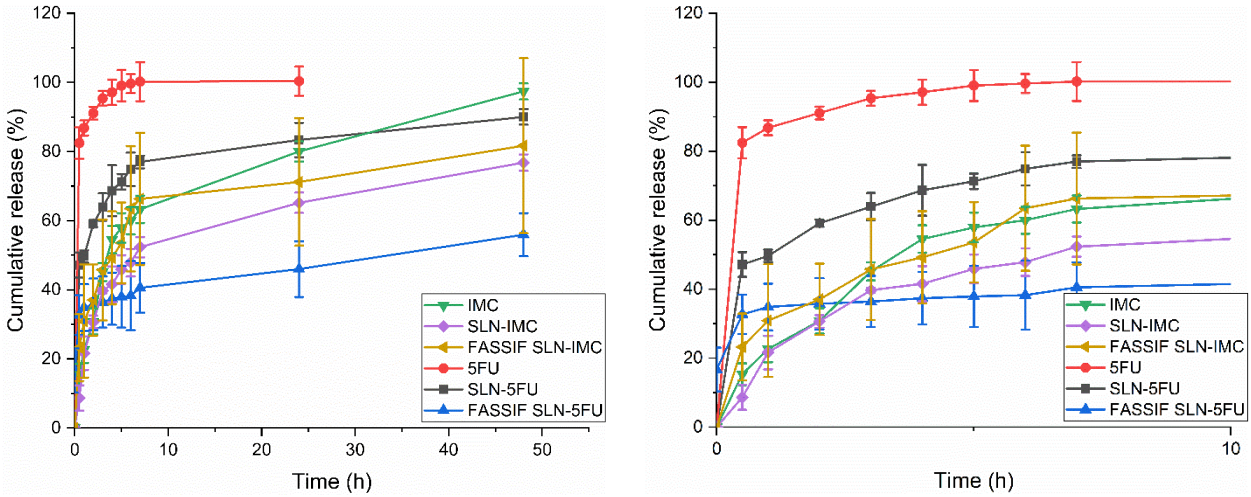


Figure 9: Drug release from the self-assembled SLNs in pH 6.8 PBS and FASSIF, showing the **(a)** full time-course of the experiment and **(b)** first 10 h (mean ± S.D. from three independent experiments).

The transit times of the small intestine and colon are around 2.5-3 h and 30-40 h respectively (Camilleri et al., 1989; Degen and Phillips, 1996; Metcalf et al., 1987), meaning that maximum drug release would be reached while the formulations are still located in the intestinal tract after oral administration. The uptake and retention of the SLNs in tumour tissue should be augmented by the enhanced permeation and retention (EPR) effect, giving them ample time to free their drug cargo (Yassin et al., 2010). Other approaches to increase the delivery of the SLNs to cancer tissues such as targeting ligands or pH sensitive systems could also be applied (Kim et al., 2015; Tran et al., 2015). In order to ensure that the SLNs reach the colon intact, an enteric coated capsule can be used.

### *3.5* In vitro *cell assays*

#### 3.5.1 Permeation

Permeation of the SLNs was explored using Caco-2 cells. The minimum inhibitory concentrations ($IC_{50}$) were first determined and found to be 7.8 mM for IMC and 1.7 mM for 5-FU. Permeation experiments were performed below these $IC_{50}$ values, at 0.2 mM. The SLNs containing IMC did not appear to permeate through the cell layer: no drug was found in the receiver compartment, and only around 5 % of the initial dose was found in the donor compartment after 2 h. At the end of the permeation study, the buffer in the donor compartment was discarded and the cell monolayer was lysed. Analysis of the lysate showed that approximately 78 % of the IMC from SLN-IMC was present in the cell monolayer. Similarly, around 62 % of the 5-FU from SLN-5FU was found in the cell monolayer and approximately 12 % in the acceptor compartment. In contrast, the percentage of pure IMC in the acceptor compartment was 54 %, while for 5-FU the donor compartment contained 71 % of the drug content. Less than 8 % of IMC or 5-FU was found in the cell monolayer when they were administered in their pure forms.

Assessment of the permeation of pure IMC resulted in a Papp value of $11.6 \times 10^{6}$ cm $s^{-1}$, typical for biopharmaceutical classification system class II (BCS II) drugs and confirming the high permeability of

IMC (Lee et al., 2017). In contrast, the 5-FU Papp value was 0.10 $x10^{6}$ cm $s^{-1}$, consistent with the literature (which shows 5-FU to have poor permeability in the Caco-2 monolayer model) (Buur et al., 1996). The SLNs prepared in this work thus accumulate in the cells, while IMC permeates and 5-FU remains in the donor compartment. The SLNs hence have significant advantages over either drug alone. If the IMC were to permeate through tumour cells and reach the systemic circulation, unwanted side effects could arise; the SLNs offer an alternative to preclude this. 5-FU alone does not effectively permeate, meaning that it may pass through the body without exerting a pharmacological effect. The SLNs enable both IMC and 5-FU to be effectively localised in cancer cells, ideal for the treatment of tumours.

Average transepithelial resistance (TEER) values were measured at the end of the permeation experiment to verify the integrity of the monolayer. The average values for the control (untreated) Caco-2 cell monolayer before and after the permeation experiment were 395.1 ± 46.6 Ω $cm^2$ and 382.0 ± 38.2 Ω $cm^2$, respectively. The values for SLN-IMC after the experiment were 360.9 ± 18.5 Ω $cm^2$ and for SLN-5FU 368.1 ± 6.8 Ω $cm^2$. It is clear that the SLNs did not have any effect on the integrity of the monolayer, thus demonstrating their low toxicity at the concentrations used for this experiment.

### 3.5.2 Viability

To evaluate the ability of the formulations to kill cancerous cells, Caco-2 cells were exposed to the SLNs for 48 h, using the $IC_{50}$ of each drug. The viability values obtained were compared to the pure drugs (Figure 10(a)). SLN-IMC and SLN-5FU do not show any significant differences compared to the drug alone, with cell viabilities of 58.2 ± 7.3% and 53.9 ± 7.2%, respectively. This indicates that the SLNs are as effective in causing the death of cancerous cells as the pure drug. Similar results were seen with human dermal fibroblasts (Figure 10(b)). This indicates that the SLNs are not selective in

their activity, as would be expected since they are not functionalised with targeting ligands. However, it does appear that the 5-FU loaded SLNs are less toxic to healthy cells than the pure drug.

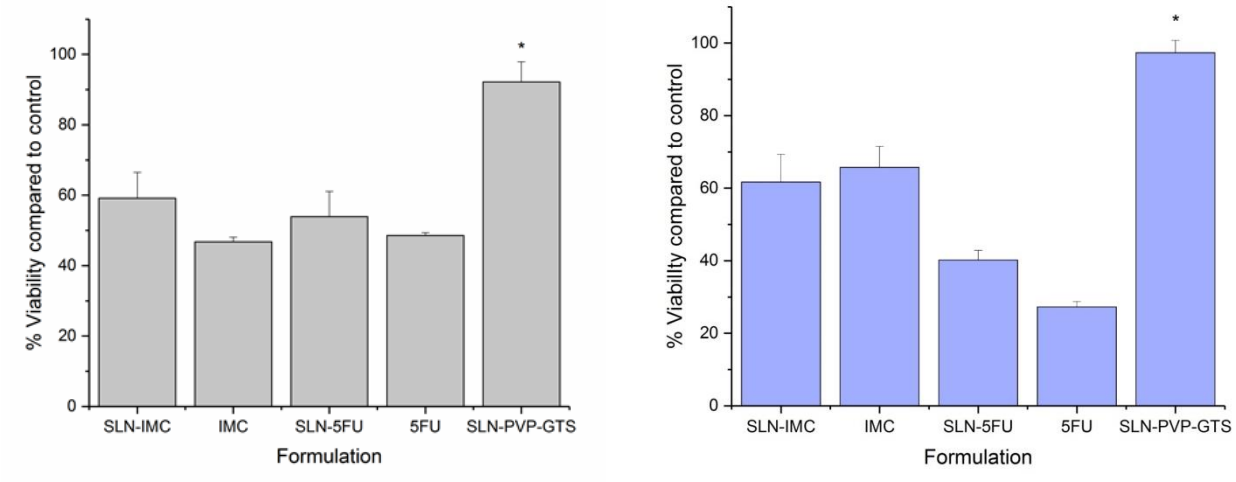


**(a)** **(b)**

Figure 10: (a) Caco-2 and (b) HDF cell viability in the presence of pure 5-FU and IMC and the drug-loaded SLNs, determined using the Alamar Blue assay. Values represent mean ± S.D. from three independent experiments with three replicates per experiment. Experiments were performed using the Caco-2 $IC_{50}$ concentration of each drug. SLNs comprising only PVP and GTS gave results significantly different to those obtained with all other formulations (* denotes $p < 0.05$).

### *3.6 SLN stability*

One of the major issues in the use of SLNs is their long-term storage stability. The stability of SLN-IMC and SLN-5FU was thus assessed in terms of their hydrodynamic diameters after 6 months of storage at room temperature. As shown in Figure 11, while the aged suspensions of SLNs show significant changes in particle size, SLNs assembled from spray dried particles aged for 6 months have virtually the same size as those assembled immediately after spray drying. In contrast, the literature reports instability of SLN suspensions of linalool over 40 days of storage (Pereira et al., 2018) and amphotericin B after 60 days storage (Santiago et al., 2018). The poor stability of SLN suspensions

arises from gelation and recrystallization of the lipid phase (Siekmann and Westesen, 1994), and by storing "proto-SLNs" in the form of spray dried particles we are able to avoid these issues.

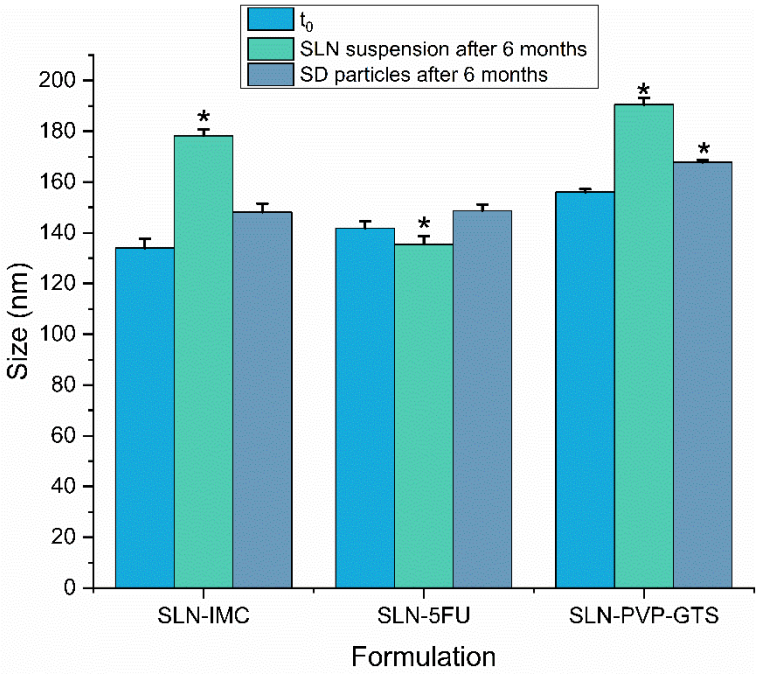


Figure 11: The results of stability studies performed for 6 months at room temperature. Data are shown from 3 independent experiments as mean ± S.D. * denotes $p < 0.05$ with respect to those obtained at the start of the experiment (t0).

## 4. Conclusions

Spray dried poly(vinylpyrrolidone) microparticles loaded with a drug and glyceryl tristearate have been shown to act as templates for the self-assembly of drug-loaded solid lipid nanoparticles (SLNs). The SLNs form upon addition of the spray dried particles to water, rather than during the spray-drying process itself. The SLNs provide a non-toxic delivery platform for both hydrophobic (indomethacin) and hydrophilic (5-fluorouracil) drugs. They have sustained release properties, and their drug cargo is seen to accumulate inside cancer cells. The SLN formulations are as efficacious as the pure drug in terms of their cytotoxicity. This work represents a novel alternative approach to the fabrication of SLNs. Because the SLNs are assembled from spray-dried microparticles on demand, the problems of instability upon storage which commonly arise with SLN formulations are obviated.

## 5. Conflicts of interest

There are no conflicts to declare.

## 6. Acknowledgements

BSV gratefully thanks CONACyT for the provision of a PhD studentship, and MM the Engineering and Physical Sciences Research Council (EPSRC) for PhD funding through the Centre for Doctoral Training in Advanced Therapeutics & Nanomedicines (EP/L01646X/1). GP would also like to thank the EPSRC (EP/M014649/1) and UCL (Excellence Fellowship) for financial support.

## 7. References

Ali, H., Prasad Verma, P.R., Dubey, S.K., Venkatesan, J., Seo, Y., Kim, S.-K., Singh, S.K., 2017. In vitro-in vivo and pharmacokinetic evaluation of solid lipid nanoparticles of furosemide using Gastroplus[trade mark sign]. RSC Advances 7, 33314-33326.

Buur, A., Trier, L., Magnusson, C., Artursson, P., 1996. Permeability of 5-fluorouracil and prodrugs in Caco-2 cell monolayers. International Journal of Pharmaceutics 129, 223-231.

Camilleri, M., Colemont, L.J., Phillips, S.F., Brown, M.L., Thomforde, G.M., Chapman, N., Zinsmeister, A.R., 1989. Human gastric emptying and colonic filling of solids characterized by a new method. Am J Physiol 257, G284-290.

Chen, D.B., Yang, T.Z., Lu, W.L., Zhang, Q., 2001. In vitro and in vivo study of two types of long-circulating solid lipid nanoparticles containing paclitaxel. Chem Pharm Bull (Tokyo) 49, 1444-1447.

Das, S., Chaudhury, A., 2011. Recent Advances in Lipid Nanoparticle Formulations with Solid Matrix for Oral Drug Delivery. AAPS PharmSciTech 12, 62-76.

Degen, L.P., Phillips, S.F., 1996. Variability of gastrointestinal transit in healthy women and men. Gut 39, 299-305.

Démuth, B., Farkas, A., Pataki, H., Balogh, A., Szabó, B., Borbás, E., Sóti, P.L., Vigh, T., Kiserdei, É., Farkas, B., Mensch, J., Verreck, G., Van Assche, I., Marosi, G., Nagy, Z.K., 2016. Detailed stability investigation of amorphous solid dispersions prepared by single-needle and high speed electrospinning. International Journal of Pharmaceutics 498, 234-244.

Du, B., Yan, Y., Li, Y., Wang, S., Zhang, Z., 2010. Preparation and passive target of 5-fluorouracil solid lipid nanoparticles. Pharm Dev Technol 15, 346-353.

Dupeyrón, D., Kawakami, M., Ferreira, A.M., Cáceres-Vélez, P.R., Rieumont, J., Azevedo, R.B., Carvalho, J.C.T., 2013. Design of indomethacin-loaded nanoparticles: effect of polymer matrix and surfactant. International Journal of Nanomedicine 8, 3467-3477.

Evans, D.F., Pye, G., Bramley, R., Clark, A.G., Dyson, T.J., Hardcastle, J.D., 1988. Measurement of gastrointestinal pH profiles in normal ambulant human subjects. Gut 29, 1035-1041.

Farkas, B., Balogh, A., Cselko, R., Molnar, K., Farkas, A., Borbas, E., Marosi, G., Nagy, Z.K., 2019. Corona alternating current electrospinning: A combined approach for increasing the productivity of electrospinning. International Journal of Pharmaceutics 561, 219-227.

Fatnassi, M., Tourné-Péteilh, C., Cacciaguerra, T., Dieudonné, P., Devoisselle, J.-M., Alonso, B., 2010. Tuning nanophase separation and drug delivery kinetics through spray drying and self-assembly. New Journal of Chemistry 34, 607.

Foley, P.J., Pippin, J.A., Smolock, C.J., Drebin, J.A., 2008. Growth inhibitory effects of indomethacin on human colon cancer cells are mediated, in-part, by effects on beta-catenin. Journal of the American College of Surgeons 207, S99.

Hippalgaonkar, K., Adelli, G.R., Hippalgaonkar, K., Repka, M.A., Majumdar, S., 2013. Indomethacin-Loaded Solid Lipid Nanoparticles for Ocular Delivery: Development, Characterization, and In Vitro Evaluation. Journal of Ocular Pharmacology and Therapeutics 29, 216-228.

Hull, M.A., Gardner, S.H., Hawcroft, G., 2003. Activity of the non-steroidal anti-inflammatory drug indomethacin against colorectal cancer. Cancer Treatment Reviews 29, 309-320.

Kalantarian, P., Najafabadi, A.R., Haririan, I., Vatanara, A., Yamini, Y., Darabi, M., Gilani, K., 2010. Preparation of 5-fluorouracil nanoparticles by supercritical antisolvents for pulmonary delivery. International Journal of Nanomedicine 5, 763-770.

Kang, K.W., Chun, M.-K., Kim, O., Subedi, R.K., Ahn, S.-G., Yoon, J.-H., Choi, H.-K., 2010. Doxorubicin-loaded solid lipid nanoparticles to overcome multidrug resistance in cancer therapy. Nanomedicine: Nanotechnology, Biology and Medicine 6, 210-213.

Kim, J.-H., Kim, Y., Bae, K.H., Park, T.G., Lee, J.H., Park, K., 2015. Tumor-Targeted Delivery of Paclitaxel Using Low Density Lipoprotein-Mimetic Solid Lipid Nanoparticles. Molecular Pharmaceutics 12, 1230-1241.

Kumar, S., Randhawa, J.K., 2015. Solid lipid nanoparticles of stearic acid for the drug delivery of paliperidone. RSC Advances 5, 68743-68750.
Lee, J.B., Zgair, A., Taha, D.A., Zang, X., Kagan, L., Kim, T.H., Kim, M.G., Yun, H.Y., Fischer, P.M., Gershkovich, P., 2017. Quantitative analysis of lab-to-lab variability in Caco-2 permeability assays. Eur J Pharm Biopharm 114, 38-42.
Lee, M.K., Lim, S.J., Kim, C.K., 2007. Preparation, characterization and in vitro cytotoxicity of paclitaxel-loaded sterically stabilized solid lipid nanoparticles. Biomaterials 28, 2137-2146.
Liu, W., Wu, W.D., Selomulya, C., Chen, X.D., 2011. Facile Spray-Drying Assembly of Uniform Microencapsulates with Tunable Core–Shell Structures and Controlled Release Properties. Langmuir 27, 12910-12915.
Lutton, E.S., 1945. The Polymorphism of Tristearin and Some of its Homologs. Journal of the American Chemical Society 67, 524-527.
Mehnert, W., Mäder, K., 2001. Solid lipid nanoparticles: Production, characterization and applications. Advanced Drug Delivery Reviews 47, 165-196.
Mehnert, W., Mäder, K., 2012. Solid lipid nanoparticles: Production, characterization and applications. Advanced Drug Delivery Reviews 64, 83-101.
Metcalf, A.M., Phillips, S.F., Zinsmeister, A.R., MacCarty, R.L., Beart, R.W., Wolff, B.G., 1987. Simplified assessment of segmental colonic transit. Gastroenterology 92, 40-47.
Mukherjee, S., Ray, S., Thakur, R.S., 2009. Solid Lipid Nanoparticles: A Modern Formulation Approach in Drug Delivery System. Indian Journal of Pharmaceutical Sciences 71, 349-358.
Müller, R.H., Mäder, K., Gohla, S., 2000. Solid lipid nanoparticles (SLN) for controlled drug delivery – a review of the state of the art. European Journal of Pharmaceutics and Biopharmaceutics 50, 161-177.
Muller, R.H., Mehnert, W., Lucks, J.S., Schwarz, C., Zur Muhlen, A., Weyhers, H., Freitas, C., Ruhl, D., 1995. Solid lipid nanoparticles (SLN) - An alternative colloidal carrier system for controlled drug delivery. European Journal of Pharmaceutics and Biopharmaceutics 41, 62-69.
Nassim, M.A., Shirazi, F.H., Cripps, C.M., Veerasinghan, S., Molepo, M.J., Obrocea, M., Redmond, D., Bates, S., Fry, D., Stewart, D.J., Goel, R., 2002. An HPLC method for the measurement of 5-fluorouracil in human plasma with a low detection limit and a high extraction yield. Int J Mol Med 10, 513-516.
Newman, A., 2015. Pharmaceutical Amorphous Solid Dispersions. Wiley.
Pansare, V.J., Rawal, A., Goodwin, A., Beyerinck, R., Prud'homme, R.K., Friesen, D.T., Grass, M., Muske-Dukes, A., Vodak, D.T., 2018. Millisecond Self-Assembly of Stable Nanodispersed Drug Formulations. Molecular Pharmaceutics 15, 495-507.
Pereira, I., Zielińska, A., Ferreira, N.R., Silva, A.M., Souto, E.B., 2018. Optimization of linalool-loaded solid lipid nanoparticles using experimental factorial design and long-term stability studies with a new centrifugal sedimentation method. International Journal of Pharmaceutics 549, 261-270.
Poozesh, S., Bilgili, E., 2019. Scale-up of pharmaceutical spray drying using scale-up rules: A review. International Journal of Pharmaceutics 562, 271-292.
Salminen, H., Ankenbrand, J., Zeeb, B., Badolato Bönisch, G., Schäfer, C., Kohlus, R., Weiss, J., 2019. Influence of spray drying on the stability of food-grade solid lipid nanoparticles. Food Research International 119, 741-750.
Santiago, R.R., Gyselle de Holanda e Silva, K., Dantas dos Santos, N., Genre, J., Freitas de Oliveira Lione, V., Silva, A.L., Marcelino, H.R., Gondim, A.D., Tabosa do Egito, E.S., 2018. Nanostructured lipid carriers containing Amphotericin B: Development, in vitro release assay, and storage stability. Journal of Drug Delivery Science and Technology 48, 372-382.
Siekmann, B., Westesen, K., 1994. Thermoanalysis of the recrystallization process of melt-homogenized glyceride nanoparticles. Colloids and Surfaces B: Biointerfaces 3, 159-175.
Singh, S.K., Jalali, A.F., Aldén, M., 1999a. Modulated temperature differential scanning calorimetry for examination of tristearin polymorphism: 2. Isothermal crystallization of metastable forms. Journal of the American Oil Chemists' Society 76, 507-510.
Singh, S.K., Jalali, A.F., Aldén, M., 1999b. Modulated temperature differential scanning calorimetry for examination of tristearin polymorphism: I. Effect of operational parameters. Journal of the American Oil Chemists' Society 76, 499-505.
Suhendi, A., Nandiyanto, A.B.D., Munir, M.M., Ogi, T., Gradon, L., Okuyama, K., 2013. Self-Assembly of Colloidal Nanoparticles Inside Charged Droplets during Spray-Drying in the Fabrication of Nanostructured Particles. Langmuir 29, 13152-13161.
Takeuchi, H., Nagira, S., Yamamoto, H., Kawashima, Y., 2005. Solid dispersion particles of amorphous indomethacin with fine porous silica particles by using spray-drying method. Int J Pharm 293, 155-164.
Tran, T.H., Ramasamy, T., Choi, J.Y., Nguyen, H.T., Pham, T.T., Jeong, J.-H., Ku, S.K., Choi, H.-G., Yong, C.S., Kim, J.O., 2015. Tumor-targeting, pH-sensitive nanoparticles for docetaxel delivery to drug-resistant cancer cells. International Journal of Nanomedicine 10, 5249-5262.
Tsvetkova, B.P.I.Z., A.; Peikov, P, 2012. High Performance Liquid Chromatographic Assay of Indomethacin and its Related Substances in Tablet Dosage Form. Int. J. Pharm. Pharm. Sci. 4 (Supplement 3), 549-552.
Valtera, J., Kalous, T., Pokorny, P., Batka, O., Bilek, M., Chvojka, J., Mikes, P., Kostakova, E.K., Zabka, P., Ornstova, J., Beran, J., Stanishevsky, A., Lukas, D., 2019. Fabrication of dual-functional composite yarns with a nanofibrous envelope using high throughput AC needleless and collectorless electrospinning. Scientific Reports 9.
Vass, P., Demuth, B., Farkas, A., Hirsch, E., Szabo, E., Nagy, B., Andersen, S.K., Vigh, T., Verreck, G., Csontos, I., Marosi, G., Nagy, Z.K., 2019. Continuous alternative to freeze drying: Manufacturing of cyclodextrin-based reconstitution powder from aqueous solution using scaled-up electrospinning. Journal of Controlled Release 298, 120-127.
Vertzoni, M., Dressman, J., Butler, J., Hempenstall, J., Reppas, C., 2005. Simulation of fasting gastric conditions and its importance for the in vivo dissolution of lipophilic compounds. European Journal of Pharmaceutics and Biopharmaceutics 60, 413-417.
Vieira, A.C., Chaves, L.L., Pinheiro, M., Ferreira, D., Sarmento, B., Reis, S., 2016. Design and statistical modeling of mannose-decorated dapsone-containing nanoparticles as a strategy of targeting intestinal M-cells. Int J Nanomedicine 11, 2601-2617.
Wang, D., DuBois, R.N., 2006. Prostaglandins and cancer. Gut 55, 115-122.

618 Xia, D., Shrestha, N., van de Streek, J., Mu, H., Yang, M., 2016. Spray drying of fenofibrate loaded nanostructured lipid carriers. Asian
619 Journal of Pharmaceutical Sciences 11, 507-515.
620 Yang, S., Zhu, J., Lu, Y., Liang, B., Yang, C., 1999. Body distribution of camptothecin solid lipid nanoparticles after oral administration.
621 Pharm Res 16, 751-757.
622 Yassin, A.E.B., Anwer, M.K., Mowafy, H.A., El-Bagory, I.M., Bayomi, M.A., Alsarra, I.A., 2010. Optimization of 5-flurouracil solid-lipid
623 nanoparticles: a preliminary study to treat colon cancer. International Journal of Medical Sciences 7, 398-408.
624 Yu, D.-G., Williams, G.R., Yang, J.-H., Wang, X., Yang, J.-M., Li, X.-Y., 2011a. Solid lipid nanoparticles self-assembled from
625 electrosprayed polymer-based microparticles. J Mater Chem 21, 15957-15961.
626 Yu, D.-G., Williams, G.R., Yang, J.-H., Wang, X., Yang, J.-M., Li, X.-Y., 2011b. Solid lipid nanoparticles self-assembled from
627 electrosprayed polymer-based microparticles. Journal of Materials Chemistry 21, 15957.
628 Yuan, Q., Han, J., Cong, W., Ge, Y., Ma, D., Dai, Z., Li, Y., Bi, X., 2014. Docetaxel-loaded solid lipid nanoparticles suppress breast cancer
629 cells growth with reduced myelosuppression toxicity. Int J Nanomedicine 9, 4829-4846.
630 Ziaee, A., Albadarin, A.B., Padrela, L., Femmer, T., O'Reilly, E., Walker, G., 2019. Spray drying of pharmaceuticals and
631 biopharmaceuticals: Critical parameters and experimental process optimization approaches. European Journal of Pharmaceutical
632 Sciences 127, 300-318.
633